LA-UR -83-3451

CONF-831255--1

Los Alamos National Laboratory is operated by the University of California for the United States Department of Energy under contract W-7405-ENG-36

LA-UR--83-3451

DE84 003813

TITLE A HYDROGEN MIXING STUDY (HMS) IN LWR TYPE CONTAINMENTS

AUTHOR(S) John R. Travis

SUBMITTED TO IAEA Specialists Meeting/Workshop on Hydrogen Behaviour and Control and Related Containment Loading Aspects
12-16 December 1983
Vienna, Austria

MASTER

Los Alamos Los Alamos National Laboratory
Los Alamos, New Mexico 87545

FORM NO 836 R4
ST NO 2629 5/81

A HYDROGEN MIXING STUDY (HMS) IN LWR TYPE CONTAINMENTS

J. R. Travis
Theoretical Division, Group T-3
University of California
Los Alamos National Laboratory
Los Alamos, NM 87545

ABSTRACT

A numerical technique has been developed for calculating the full three-dimensional time-dependent Navier-Stokes equations with multiple species transport. The method is a modified form of the Implicit Continuous-fluid Eulerian (ICE) technique to solve the governing equations for low Mach number flows where pressure waves and local variations in compression and expansion are not significant. Large density variations, due to thermal and species concentration gradients, are accounted for without the restrictions of the classical Boussinesq approximation. Calculations of the EPRI/HEDL standard problems verify the feasibility of using this finite-difference technique for analyzing hydrogen mixing within LWR containments.

I. INTRODUCTION

During and after a loss-of-coolant accident in a light-water reactor, water may be decomposed by chemical reactions and radiolysis to release gaseous hydrogen. Should hydrogen be released, two deleterious effects could occur. The noncondensable gas can increase the containment pressure. In sufficient amounts, the hydrogen could burn in the presence of air, causing considerable loads on the containment walls or harm to crucial control devices. Each effect represents an additional safety risk. To better assess the problem, we have developed a multidimensional fluid dynamics finite-difference code to calculate the details of hydrogen transport through containment structures.

This detailed model of the full three-dimensional time-dependent Navier-Stokes equations with species transport is solved by a variant of the Implicit Continuous-fluid Eulerian (ICE)[1] technique. We make use of the idea that for low-speed flows pressure wave propagation need not be resolved in detail and therefore the local fluid density is a function of the average fluid pressure, local temperature, and relative concentrations of available species. This further allows accurate representation of flows driven by large density variations for which the Boussinesq approximation may not provide sufficient accuracy.[2]

Ultimately this detailed model, together with relevant experimental data, will help to benchmark existing hydrogen migration systems codes that are necessarily based on simpler models. This paper presents the governing equations, develops the solution procedure, and presents numerical results for comparison of experimental results in the three-dimensional geometry of the EPRI/HEDL standard problems.[3]

II. MATHEMATICAL DESCRIPTION

The partial-differential equations that govern the fluid dynamics and species transport are presented in this section. They are written in cylindrical coordinates; however, the equations for plane coordinates are easily obtained by setting the radial distance r equal to unity and the terms with the β multiplier equal to zero; i.e., $\beta = 1$ for cylindrical coordinates and $\beta = 0$ for planar coordinates.

A. The Mixture Equations

The mixture mass conservation equation is

$$\frac{\partial \rho}{\partial t} + \nabla\cdot(\rho\bar{u}) = \sum_{\alpha=1}^{3} S_\alpha \quad , \tag{1}$$

where

$\rho = \sum_{\alpha=1}^{3} \rho'_\alpha$; ρ'_α = macroscopic density of the individual species (air, steam, or hydrogen),

$\bar{u}$ = mass-average velocity vector, and

S_α = mass source (+) and/or sink (-) of species α per unit volume and time.

The mixture momentum conservation equations are given by

$$\frac{\partial(\rho\bar{u})}{\partial t} + \nabla\cdot(\rho\bar{\bar{u}}\bar{\bar{u}}) = -\nabla p + \nabla\cdot\bar{\bar{\sigma}} + \hat{\rho}\bar{g} + \bar{M} \quad , \tag{2}$$

where

p = pressure,

$\bar{\bar{\sigma}}$ = viscous stress tensor,

$\hat{\rho}$ = local density relative to the average density (see next section), and

$\bar{M}$ = momentum source vector per unit volume and time (see Sec. IV).

In these equations, the viscous force per unit volume and time, $\nabla\cdot\bar{\sigma}$, is given for the

r- or x-component

$$\nabla\cdot\bar{\sigma} = \frac{1}{r}\frac{\partial}{\partial r}(r\,\sigma_{rr}) + \frac{1}{r}\frac{\partial}{\partial\theta}\sigma_{r\theta} - \beta\frac{\sigma_{\theta\theta}}{r} + \frac{\partial}{\partial z}\sigma_{rz} \quad ,$$

θ- or y-component

$$\nabla\cdot\bar{\sigma} = \frac{1}{r^2}\frac{\partial}{\partial r}(r^2\,\sigma_{r\theta}) + \frac{1}{r}\frac{\partial}{\partial\theta}\sigma_{\theta\theta} + \frac{\partial}{\partial z}\sigma_{\theta z} \quad , \text{ and}$$

z-component

$$\nabla\cdot\bar{\sigma} = \frac{1}{r}\frac{\partial}{\partial r}(r\,\sigma_{rz}) + \frac{1}{r}\frac{\partial}{\partial\theta}\sigma_{\theta z} + \frac{\partial}{\partial z}\sigma_{zz} \quad .$$

The components of the viscous stress tensor are defined as follows:

$$\sigma_{rr} = 2\mu\frac{\partial u}{\partial r} + \lambda\nabla\cdot\bar{u} \quad ,$$

$$\sigma_{\theta\theta} = 2\mu\left(\frac{1}{r}\frac{\partial w}{\partial\theta} + \beta\frac{u}{r}\right) + \lambda\nabla\cdot\bar{u} \quad ,$$

$$\sigma_{zz} = 2\mu\frac{\partial v}{\partial z} + \lambda\nabla\cdot\bar{u} \quad ,$$

$$\sigma_{r\theta} = \sigma_{\theta r} = \mu\left[r\frac{\partial}{\partial r}\left(\frac{w}{r}\right) + \frac{1}{r}\frac{\partial u}{\partial\theta}\right] \quad ,$$

$$\sigma_{\theta z} = \sigma_{z\theta} = \mu\left[\frac{\partial w}{\partial z} + \frac{1}{r}\frac{\partial v}{\partial\theta}\right] \quad , \text{ and}$$

$$\sigma_{zr} = \sigma_{rz} = \mu\left[\frac{\partial v}{\partial r} + \frac{\partial u}{\partial z}\right] \quad ,$$

where μ and λ are the first and second coefficients of viscosity, respectively, and

$$\nabla\cdot\bar{u} = \frac{1}{r}\frac{\partial}{\partial r}(ru) + \frac{1}{r}\frac{\partial w}{\partial \theta} + \frac{\partial v}{\partial z} \quad .$$

The mixture internal energy equation is

$$\frac{\partial}{\partial t}(\rho I) + \nabla\cdot(\rho I\bar{u}) = \nabla\cdot(K\nabla T) + Q \quad , \tag{3}$$

where

I = mixture specific internal energy,
K = thermal conductivity,
T = mixture temperature, and
Q = energy source and/or sink per unit volume and time.

We assume viscous dissipation is negligible for the low-speed flows of interest.

The equation-of-state for the average fluid pressure P_o is given by the ideal gas mixture equation

$$P_o = T\sum_{\alpha=1}^{3}(\gamma_\alpha - 1)(C_v)_\alpha \rho'_\alpha \quad , \tag{4}$$

where γ_α is the ratio of specific heats for species α and $(C_v)_\alpha$ is the specific heat at constant volume for species α.

B. The Species Transport Equations

The dynamics of the individual species are determined by

$$\frac{\partial \rho'_\alpha}{\partial t} + \nabla\cdot(\rho'_\alpha\bar{u}) = S_\alpha \quad . \tag{5}$$

Summing Eq. (5) over all species results in the mixture mass Eq. (1).

III. THE FINITE DIFFERENCE EQUATIONS AND SOLUTION PROCEDURE

Equations (1) - (3) and (5) are written in finite difference form for their numerical solution. The nonlinear finite-difference equations are then solved

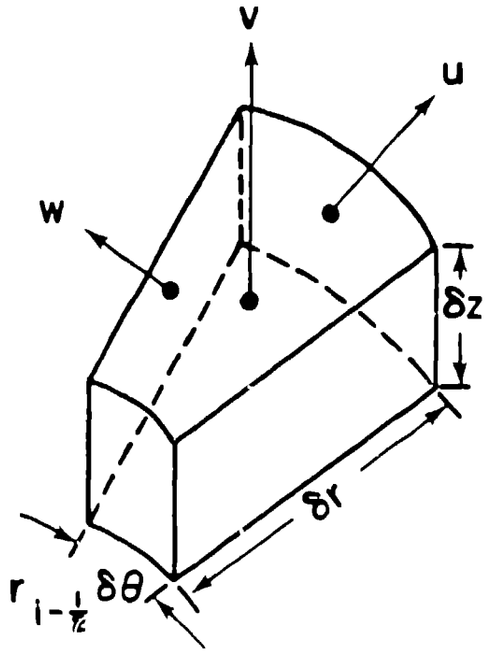

Fig. 1.
Locations of velocity components for a typical cell in cylindrical geometry.

iteratively using a point relaxation method. Since we are interested in low-speed flows where the propagation of pressure waves need not be resolved, we are therefore utilizing a modified ICE[1] solution technique where the species densities are functions of the global or compartment pressure, and not of the local pressure. Time-dependent solutions can be obtained in one, two, and three space dimensions in plane and in cylindrical geometries. The geometric region of interest is divided into many finite-size, space-fixed zones called computational cells that collectively form the computing mesh. Figure 1 shows a typical computational cell with the velocities centered on the cell boundaries. All other quantities, such as I, p and (ρ'_a)'s, are positioned at the cell-center designated (i,j,k). The finite-difference equations for the quantities at time t = (n+1)δt form a system of coupled, non-linear algebraic equations. The equations are given below and the solution method follows.

For the problems of interest (See Sec. IV), the source/sink terms in the species transport equations are:

(1) Air (a); $S_a = 0$;

(2) Hydrogen or helium (h); S_h = hydrogen or helium mass per unit volume and time in the jet; and

(3) Steam(s), $S_s - C_s$ = (steam mass per unit volume and time in the jet) - (condensation mass per unit volume and time).

The sources of hydrogen or helium and steam are specified by the experiment; however, the condensation rate must be modeled. We propose the simple but effective relationship, based on the assumption of local equilibrium,

$$C_s = R'\rho'_s(\text{local steam density}) - \rho'_{sat}(T)]$$

where

$\rho'_{sat}(T)$ = saturation steam density at temperature T,

$R = 10^{10}$ /s for ρ'_s(local steam density) $> \rho'_{sat}(T)$, or

$R = 0$, otherwise.

For cell i,j,k we will implicitly solve for the n+1 steam density, $(\rho'_s)^{n+1}_{i,j,k}$, by writing

$$(C_s)^{n+1}_{i,j,k} = R[(\rho'_s)^{n+1}_{i,j,k} - \rho'_{sat}(T^n)] \quad ,$$

which allows any degree of condensation while the numerical scheme remains stable. The steam transport equation is then written

$$(\rho'_s)^{n+1}_{i,j,k} = \{(\rho'_s)^{n}_{i,j,k} + \delta t[- \langle(\rho'_s)^{n+1}u^{n+1}r\rangle_{i,j,k}/(r_i \delta r)$$

$$- \langle(\rho'_s)^{n+1}v^{n+1}\rangle_{i,j,k}/\delta z - \langle(\rho'_s)^{n+1}w^{n+1}\rangle_{i,j,k}/(r_i \delta\theta)$$

$$+ (S_s)_{i,j,k} + R\,\rho'_{sat}(T^n)]\}/(1 + \delta t R) \quad .$$

The flux quantities, for example $\langle\rho'_s ur\rangle_{i,j,k}$, are calculated using donor-cell differencing, so that

$$\langle\rho'_s ur\rangle_{i,j,k} = u_{i+\frac{1}{2},j,k} r_{i+\frac{1}{2}} \cdot \begin{cases} (\rho'_s)_{i,j,k} & \text{if } u_{i+\frac{1}{2},j,k} > 0 \\ (\rho'_s)_{i+1,j,k} & \text{if } u_{i+\frac{1}{2},j,k} < 0 \end{cases}$$

$$- u_{i-\frac{1}{2},j,k} r_{i-\frac{1}{2}} \cdot \begin{cases} (\rho'_s)_{i-1,j,k} & \text{if } u_{i-\frac{1}{2},j,k} > 0 \\ (\rho'_s)_{i,j,k} & \text{if } u_{i-\frac{1}{2},j,k} < 0 \end{cases} \quad .$$

The transport equations for hydrogen or helium and air and the mixture mass equation are [illegible] in similar fashion.

The finite-difference representation of the mixture momentum equations is

$$(\rho u)^{n+1}_{i+\frac{1}{2},j,k} = (\widetilde{\rho u})^{n}_{i+\frac{1}{2},j,k} - \delta t\,(p^{n+1}_{i+1,j,k} - p^{n+1}_{i,j,k})/\delta r \quad , \tag{6}$$

$$(\rho v)^{n+1}_{i,j+\frac{1}{2},k} = (\widetilde{\rho v})^{n}_{i,j+\frac{1}{2},k} - \delta t\,(p^{n+1}_{i,j+1,k} - p^{n+1}_{i,j,k})/\delta z \quad , \text{ and} \tag{7}$$

$$(\rho w)^{n+1}_{i,j,k+\frac{1}{2}} = (\widetilde{\rho w})^{n}_{i,j,k+\frac{1}{2}} - \delta t\,(p^{n+1}_{i,j,k+1} - p^{n+1}_{i,j,k})/(r_i\,\delta\theta) \quad . \tag{8}$$

The momentum density quantities designated by the superscript tilde ($\widetilde{\ }$) account for the effects of momentum convection, gravity, source, and viscous stress. For example, consider

$$\begin{aligned}(\widetilde{\rho v})^{n}_{i,j+\frac{1}{2},k} = (\rho v)^{n}_{i,j+\frac{1}{2},k} + \delta t\{ &- \langle \rho^n v^n u^n r\rangle_{i,j+\frac{1}{2},k}/(r_i\,\delta r) \\ &- \langle \rho^n v^n v^n\rangle_{i,j+\frac{1}{2},k}/\delta z - \langle \rho v^n w^n\rangle_{i,j+\frac{1}{2},k}/(r_i\,\delta\theta) \\ &+ \hat{\rho}^{n}_{i,j+\frac{1}{2},k} g + (M_z)^{n}_{i,j+\frac{1}{2},k} \\ &+ [r_{i+\frac{1}{2}}(\sigma_{rz})^{n}_{i+\frac{1}{2},j+\frac{1}{2},k} - r_{i-\frac{1}{2}}(\sigma_{rz})^{n}_{i-\frac{1}{2},j+\frac{1}{2},k}]/(r_i\,\delta r) \\ &+ [(\sigma_{zz})^{n}_{i,j+1,k} - (\sigma_{zz})^{n}_{i,j,k}]/\delta z \\ &+ [(\sigma_{\theta z})^{n}_{i,j+\frac{1}{2},k+\frac{1}{2}} - (\sigma_{\theta z})^{n}_{i,j+\frac{1}{2},k-\frac{1}{2}}]/(r_i\,\delta\theta)\} \quad .\end{aligned}$$

Representing the gravity term by

$$\hat{\rho}^{n}_{i,j+\frac{1}{2},k} g = \left[\rho^{n}_{i,j+\frac{1}{2},k} - \frac{\sum_k \sum_i \rho^{n}_{i,j+\frac{1}{2},k} r_i}{\sum_k \sum_i r_i}\right] g$$

removes the necessity for resolving the hydrostatic pressure gradient, but it allows accurate representation of buoyancy forces developing from large density variations due to species concentration and temperature gradients. The momentum source (M_z) will be addressed in the next section.

The components of the viscous stress tensor are differenced in a similar manner, e.g.,

$$(\sigma_{zz})^n_{i,j+1,k} = 2\mu(v^n_{i,j+3/2,k} - v^n_{i,j+\frac{1}{2},k})/\delta z$$

$$+ \lambda[(r_{i+\frac{1}{2}}u^n_{i+\frac{1}{2},j+1,k} - r_{i-\frac{1}{2}}u^n_{i-\frac{1}{2},j+1,k})/(r_i \delta r)$$

$$+ (w^n_{i,j+1,k+\frac{1}{2}} - w^n_{i,j+1,k-\frac{1}{2}})/(r_i \delta\theta)$$

$$+ (v^n_{i,j+3/2,k} - v^n_{i,j+\frac{1}{2},k})/\delta z] \quad .$$

In the mixture internal energy equation, the source and/or sink term $Q_{i,j,k}$ is written

$$Q_{i,j,k} = (S_h I_h)^n_{i,j,k} + (S_s I_s)^n_{i,j,k} - (C_s I)^n_{i,j,k} - \frac{AH^n}{Vol_{i,j,k}} (T^{n+1}_{i,j,k} - T_w) \quad ,$$

where

I_h = internal energy of the hydrogen or helium in the source,

I_s = internal energy of the steam in the source

H = local wall heat transfer coefficient,

A = wall area, and

Vol = volume of the computational cell adjacent to the wall.

Note that in the wall heat transfer term the temperature is written at the advanced time level (n+1). This allows for a stable solution for all physical values of the heat transfer coefficient. By making use of the caloric equation-of-state

$$I = \bar{C}_v T \quad ,$$

where the average specific heat is expressed in terms of the species, densities, and constant specific heats

$$\bar{C}_v = \rho^{-1} \sum_{\alpha=1}^{3} \rho'_\alpha (C_v)_\alpha \quad ,$$

the wall heat transfer term is rewritten

$$\frac{AH^n}{Vol_{i,j,k}} \left[\frac{(\rho I)^{n+1}_{i,j,k}}{\sum_{\alpha=1}^{3} (\rho'_\alpha)^{n+1}_{i,j,k} (C_v)_\alpha} - T_w \right] \quad .$$

The finite-difference equation for the mixture specific internal energy equation is then given by

$$(\rho I)^{n+1}_{i,j,k} = \Bigg\{ (\rho I)^n_{i,j,k} + \delta t \Bigg\{ - \langle \rho^n I^n u^n r \rangle_{i,j,k} / (r_i \delta r) - \langle \rho^n I^n v^n \rangle_{i,j,k} / \delta z$$

$$- \langle \rho^n I^n w^n \rangle / (r_i \delta\theta) + [r_{i+\frac{1}{2}} K^n_{i+\frac{1}{2},j,k} (T^n_{i+1,j,k} - T^n_{i,j,k})$$

$$- r_{i-\frac{1}{2}} K^n_{i-\frac{1}{2},j,k} (T^n_{i,j,k} - T^n_{i-1,j,k})] / (r_i \delta r^2)$$

$$+ [K^n_{i,j+\frac{1}{2},k} (T^n_{i,j+1,k} - T^n_{i,j,k})$$

$$- K^n_{i,j-\frac{1}{2},k} (T^n_{i,j,k} - T^n_{i,j-1,k})] / \delta z^2$$

$$+ [K^n_{i,j,k+\frac{1}{2}} (T^n_{i,j,k+1} - T^n_{i,j,k})$$

$$- K^n_{i,j,k-\frac{1}{2}} (T^n_{i,j,k} - T^n_{i,j,k-1})] / (r_i \delta\theta)^2$$

$$+ (S_h I_h)^n_{i,j,k} + (S_s I_s)^n_{i,j,k} - (C_s I)^n_{i,j,k}$$

$$+ \frac{AH^n T_w}{Vol_{i,j,k}} \Bigg\} \Bigg\} \Bigg/ \left[1 + \frac{\delta t AH^n}{Vol_{i,j,k} \sum_{\alpha=1}^{3} (\rho'_\alpha)^{n+1}_{i,j,k} (C_v)_\alpha} \right] \quad (9)$$

The solution method starts with the calculation of S_h^n, S_s^n, $(\widetilde{\rho u})^n$, $(\widetilde{\rho v})^n$, $(\widetilde{\rho w})^n$, H^n, K^n and estimates of $\langle \rho^{n+1} u^{n+1}_r \rangle$, $\langle \rho^{n+1} v^{n+1} \rangle$, $\langle \rho^{n+1} w^{n+1} \rangle$, u^{n+1}, v^{n+1}, and w^{n+1}, are made. The solution method proceeds with the iteration phase:

(1) The $(\rho'_\alpha)^{n+1}_{i,j,k}$'s are found from the species transport equations using the latest iterates for $(\rho'_\alpha)^{n+1}$ and $\bar{u}^{n+1}$.

(2) The global or average fluid pressure, P_o^{n+1} is determined from integrating the equation-of-state (4) over the computational volume

$$\iiint_{Vol} \frac{P_o}{T} \, dVol = \iiint_{Vol} \sum_{\alpha=1}^{3} (\gamma_\alpha - 1)(C_v)_\alpha \rho'_\alpha \, dVol$$

or,

$$P_o^{n+1} = \frac{\sum\sum\sum_{ijk} r_i \sum_{\alpha=1}^{3} (\gamma_\alpha - 1)(C_v)_\alpha (\rho'_\alpha)^{n+1}_{i,j,k}}{\sum\sum\sum_{ijk} r_i / T^n_{i,j,k}} \, .$$

(3) The equation-of-state is modified slightly to find the mixture density using the $(\rho'_\alpha)^{n+1}$'s and P_o^{n+1} from steps (1) and (2)

$$\rho^{n+1}_{i,j,k} = \frac{P_o^{n+1} \sum_{\alpha=1}^{3} (\rho'_\alpha)^{n+1}_{i,j,k}}{T^n_{i,j,k} \sum_{\alpha=1}^{3} (\gamma_\alpha - 1)(C_v)_\alpha (\rho'_\alpha)^{n+1}_{i,j,k}} \, .$$

(4) With $\rho^{n+1}_{i,j,k}$ [from step (3)] and the latest iterates for $\bar{u}^{n+1}$ the residual, $D_{i,j,k}$, in the mixture mass equation is calculated

$$D_{i,j,k} = \rho^{n+1}_{i,j,k} - \rho^{n}_{i,j,k} + \delta t[\langle \rho^{n+1} u^{n+1} r \rangle_{i,j,k}/(r_i \delta r)$$

$$+ \langle \rho^{n+1} v^{n+1} \rangle_{i,j,k}/\delta z + \langle \rho^{n+1} w^{n+1} \rangle_{i,j,k}/(r_i \delta\theta)$$

$$- (S_h)^{n}_{i,j,k} - (S_s)^{n}_{i,j,k} + (C_s)^{n+1}_{i,j,k}] \quad .$$

If the convergence criterion is met, for example, $|D_{i,j,k}| < \varepsilon$ where $\varepsilon = 10^{-4}\ \rho^{n}_{i,j,k}$, then no adjustment is made to the local pressure, $p^{n+1}_{i,j,k}$, and the velocities $\bar{u}^{n+1}_{i,j,k}$ for cell (i,j,k). If the convergence criterion is met for all cells in the computational mesh, then the iteration phase of the cycle is complete.

(5) For any cell that the criterion is not met, the local pressure is changed by an amount

$$\delta p_{i,j,k} = - \frac{\Omega\ D_{i,j,k}}{\left(\frac{\partial D}{\partial p}\right)_{i,j,k}} \quad ,$$

where

$$\left(\frac{\partial D}{\partial p}\right)_{i,j,k} = \frac{2\delta t^2}{\delta r^2 + (r_i \delta\theta)^2 + \delta z^2} \quad ,$$

and Ω is a constant over-relaxation factor selected $1.0 \leq \Omega < 2.0$, and the momenta are changed as shown in Eqs. (6) - (8). The velocities are found by simply evaluating

$$u^{n+1}_{i+\frac{1}{2},j,k} = \frac{2(\rho u)^{n+1}_{i+\frac{1}{2},j,k}}{\rho^{n+1}_{i,j,k} + \rho^{n+1}_{i+1,j,k}} \quad ,$$

$$v^{n+1}_{i,j+\frac{1}{2},k} = \frac{2(\rho v)^{n+1}_{i,j+\frac{1}{2},k}}{\rho^{n+1}_{i,j,k} + \rho^{n+1}_{i,j+1,k}} \quad , \text{ and}$$

$$w^{n+1}_{i,j,k+\frac{1}{2}} = \frac{2(\rho w)^{n+1}_{i,j,k+\frac{1}{2}}}{\rho^{n+1}_{i,j,k} + \rho^{n+1}_{i,j,k+1}} \quad .$$

Steps (1) - (5) are repeated until the convergence criterion as presented in step (4) is satisfied on the entire computational mesh. After the iteration phase is complete, the specific internal energy is calculated by Eq. (9) and the computational time step is finished with the advancement of the time step.

More details of the HMS solution methodology, code description, and a listing of the code are given in Ref. (4).

IV. NUMERICAL RESULTS

This computer code was developed to analyze the EPRI/HEDL standard problems "A" and "B".[3] The standard problems A and B, tests HM-5 and HM-6 in reference 5 respectively, were proposed as a bases for comparing blind predictions of detailed hydrogen distribution in reactor-like containment compartments. In both experiments a high velocity steam-hydrogen or steam-helium jet is released into the compartment. The reader is referred to Ref. 5, which is part of these proceedings, for a detailed discussion of the experimental facility.

Figure 2 presents the discretization of the containment compartment. We have modeled the blower which provides recirculation from the upper to lower compartments as four time-dependent prescribed inflow boundary cells. These are shown on the outer circumference (R = 3.81 m) at the axial position 2.36 m $\leq$ Z $\leq$ 3.15 m and in the azimuthal positions 20° $\leq \theta \leq$ 40°, 80° $\leq \theta \leq$ 100°, 200° $\leq \theta \leq$ 220°, and 260° $\leq \theta \leq$ 280°. Flow is allowed to exit the computational mesh by the eight continuative outflow boundary cells shown on the outer circumference (R = 381 m) at the axial position 3.93 m $\leq$ Z $\leq$ 4.72 m and in the azimuthal positions 0° $\leq \theta \leq$ 20°, 40° $\leq \theta \leq$ 60°, 80° $\leq \theta \leq$ 100°, 120° $\leq \theta \leq$ 140°, 160° $\leq \theta \leq$ 180°, 200° $\leq \theta \leq$ 220°, 240° $\leq \theta \leq$ 260°, and 280° $\leq \theta \leq$ 300°. Both tests started with the compartment at 65°C and 10^5 Pa (1 bar), with test A containing nitrogen and test B containing air. Table I lists the timing of events for each test.

TABLE I. Timing of Events

Test A		Test B	
Time (minutes)	Event	Time (minutes)	Event
11.50	Recirculator blower on	4.00 (4.50)*	Recirculator blower on
11.75	Steam source on	4.75	Steam source on
12.50	Hydrogen source on	6.25	Helium source on
12.75	Nitrogen becomes saturated in recirculators	6.50	Air becomes saturated in recirculators
13.5	Hydrogen begins entering compartment through recirculators	7.00	Helium begins entering compartment through recirculators
23.75	Sources shut off	17.00	Sources shut off

*Blind calculation started at 4.00 minutes and the posttest calculation started at 4.50 minutes.

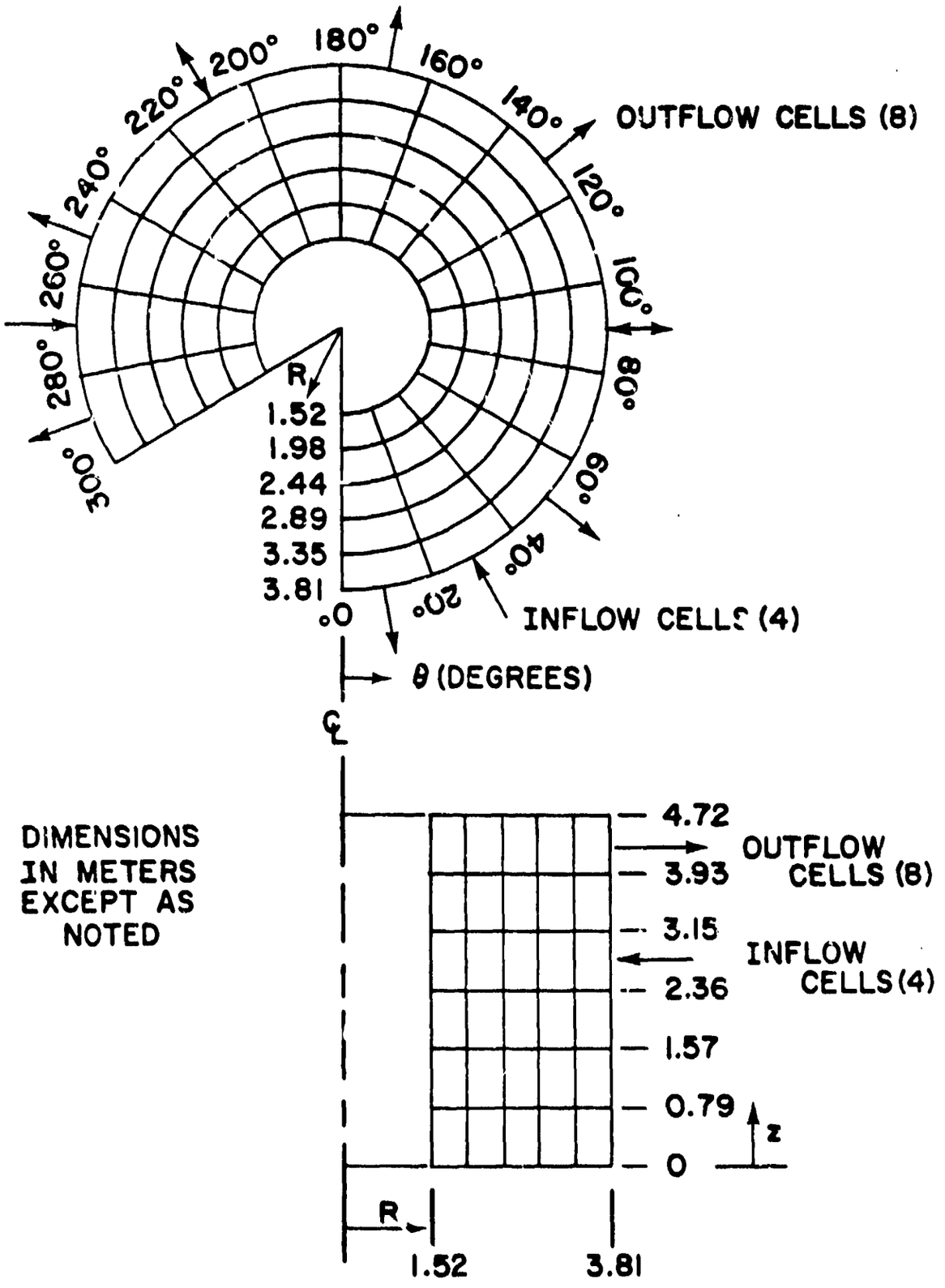

Fig. 2. HMS computing mesh for EPRI/HEDL Standard Problems A and B.

Compartment wall temperatures were assumed constant at 65°C through both tests, while time-dependent prescribed inflow data consistent with the events of Table I are tabulated in Table II.

Experiment A had a horizontal steam-hydrogen jet that was centered in the annulus at 275° at a height of 1.52 m from the floor. The average jet velocity was assumed to be 150 m/s, and it was directed inward at 60° to a radial ray, which led to a momentum source:

$$(M_r)_{R = 2.44m,\ 0.79\ m \le Z \le 1.57\ m,\ 260° \le \theta \le 280°} = -\frac{1}{2}(S_s + S_h)(150),$$

$$(M_\theta)_{2.44m \le R \le 2.89\ m,\ 0.79\ m \le Z \le 1.57\ m,\ \theta = 260°} = -0.866(S_s + S_h)(150), \text{ and}$$

$$(M_z) = 0 \quad ,$$

TABLE II. Time-Dependent Prescribed Inflow Data†

Test A		Test B	
Time (minutes)	Inlet Temperature (°C)	Time (minutes)	Inlet Temperature (°C)
0.0	35.0	0.0	35.0
8.0	35.0	4.0	35.0
10.0	35.5	7.0	42.0
13.0	40.0	10.0	43.0
18.0	53.0	11.0	46.5
21.0	57.0	16.0	52.0
23.0	58.25	17.0	52.5
24.0	56.5	20.0	49.5
32.0	53.5	29.0	46.5
35.0	52.5	31.5	46.5
46.0	51.0	32.5	48.0
60.0	50.0	70.0	47.5

Time (minutes)	Hydrogen Concentration (%)*	Time (minutes)	Helium Concentration (%)*
0.0	0.0	0.0	0.0
13.5	0.0	7.0	0.0
15.0	0.6	17.0	3.45
24.0	5.4	19.0	3.55
25.0	5.5	24.0	3.45
32.0	5.1	65.0	3.2
47.0	4.9		
70.0	4.8		

†The inlet velocity is held constant at 0.434 m/s throughout both tests.

*Hydrogen and Helium concentrations are given in volume % on a dry basis; i.e., the steam has been removed.

where the time-dependent mass sources S_s and S_h are tabulated in Table III. Experiment B had a vertical steam-helium jet that was located at 180°, 1.2 m from the floor, and 2.31 m from the compartment axis. The average jet velocity was assumed to be 80 m/s which led to a momentum source:

$$(M_r) \sim 0,$$

$$(M_\theta) = 0, \text{ and}$$

$$(M_z)_{1.98\ m \leq R \leq 2.44\ m,\ Z = 1.57\ m,\ 160° \leq \theta \leq 180°} = (S_s + S_h)(80).$$

The energy source due to the jet is calculated $S_h I_h + S_s I_s$, where $I_h = (C_v)_h T$ and $I_s = (C_v)_s T$, and T is the time-dependent jet temperature listed in Table IV. For tests A and B the mass and energy sources are associated with cells ($2.44\ m \leq R \leq 2.89\ m$, $0.79\ m \leq Z \leq 1.57\ m$, $260° \leq \theta \leq 280°$), and ($1.98 \leq R \leq 2.44\ m$, $0.79\ m \leq Z \leq 1.57\ m$, $160° \leq \theta \leq 180°$), respectively.

Intermediate values of the parameters in Tables II - IV may be found by linear interpolation.

TABLE III. Time-Dependent Mass Source

Test A

Steam Mass		Hydrogen Mass	
Time (minutes)	Flow Rate (kg/min)	Time (minutes)	Flow Rate (kg/min)
0.0	0.0	0.0	0.0
11.75	0.0	12.5	0.0
12.50	21.0	13.	0.31
14.0	24.0	23.0	0.31
23.0	24.0	23.75	0.0
23.75	0.0	60.0	0.0
60.0	0.0		

Test B

Steam Mass		Helium Mass	
Time (minutes)	Flow Rate (kg/min)	Time (minutes)	Flow Rate (kg/min)
0.0	0.0	0.0	0.0
4.75	0.0	6.25	0.0
5.50	14.5	7.0	0.405
16.0	14.5	15.25	0.405
17.0	0.0	16.0	0.94
60.0	0.0	17.0	0.0
		60.0	0.0

TABLE IV. Time-Dependent Jet Temperature

Test A		Test B	
Time (minutes)	Temperature (°C)	Time (minutes)	Temperature (°C)
10.0	108.0	2.0	110.0
16.5	101.0	7.0	96.0
18.0	103.0	12.5	96.0
18.5	124.0	17.0	124.0
19.0	130.0	18.0	113.0
20.0	133.0	19.0	109.0
21.0	136.0	21.0	107.0
23.0	140.0	60.0	94.0
24.0	140.0		
26.0	129.0		
28.0	125.0		
60.0	109.0		

In Figs. 3 and 4, we present the test data and the blind (i.e., pretest) concentration predictions for tests A and B, respectively. The curve designated "E" represents the experimental data while the curve designated "C" represents the calculation. For test A, the horizontal jet, there is total mixing throughout the compartment as evidenced by the similarity of the concentration curves and maximum concentrations at various locations in the compartment. All concentrations in this paper are reported in volume percent on a dry basis; i.e., the steam was condensed and the gas sample passed through a drying bed in the tests. Concentrations for test B, the vertical jet, are presented for the same locations as test A. Here we see a definite concentration gradient of roughly 2 to 3 concentration percent during the gas injection phase with maximum values at the compartment top and minimum values at the bottom. This gradient quickly decays to about 1% after the jet to shut off. Our blind calculations of the concentrations are seen to predict the test data very well. The blind temperature predictions were not very good as depicted in Fig. 5. We recognized this at the time,[6] but nevertheless judged our concentrations to be substantially correct. The reason that concentration is not sensitive to temperature in these tests is because the steam is mostly superheated vapor throughout the compartment.

During the posttest analysis, an error was found in the solution of the energy equation. Recalculations showed negligible change in the concentrations and good agreement with the temperatures, as shown in Fig. 6. The corrected energy equation also includes the Uchida[7] correlation for wall-heat transfer and the assumption that K = 0.

For roughly 15 minutes of physical time, these problems required between 5 and 6 hours of CDC 7600 CPU times, or about 2.5 hours of Cray CPU time.

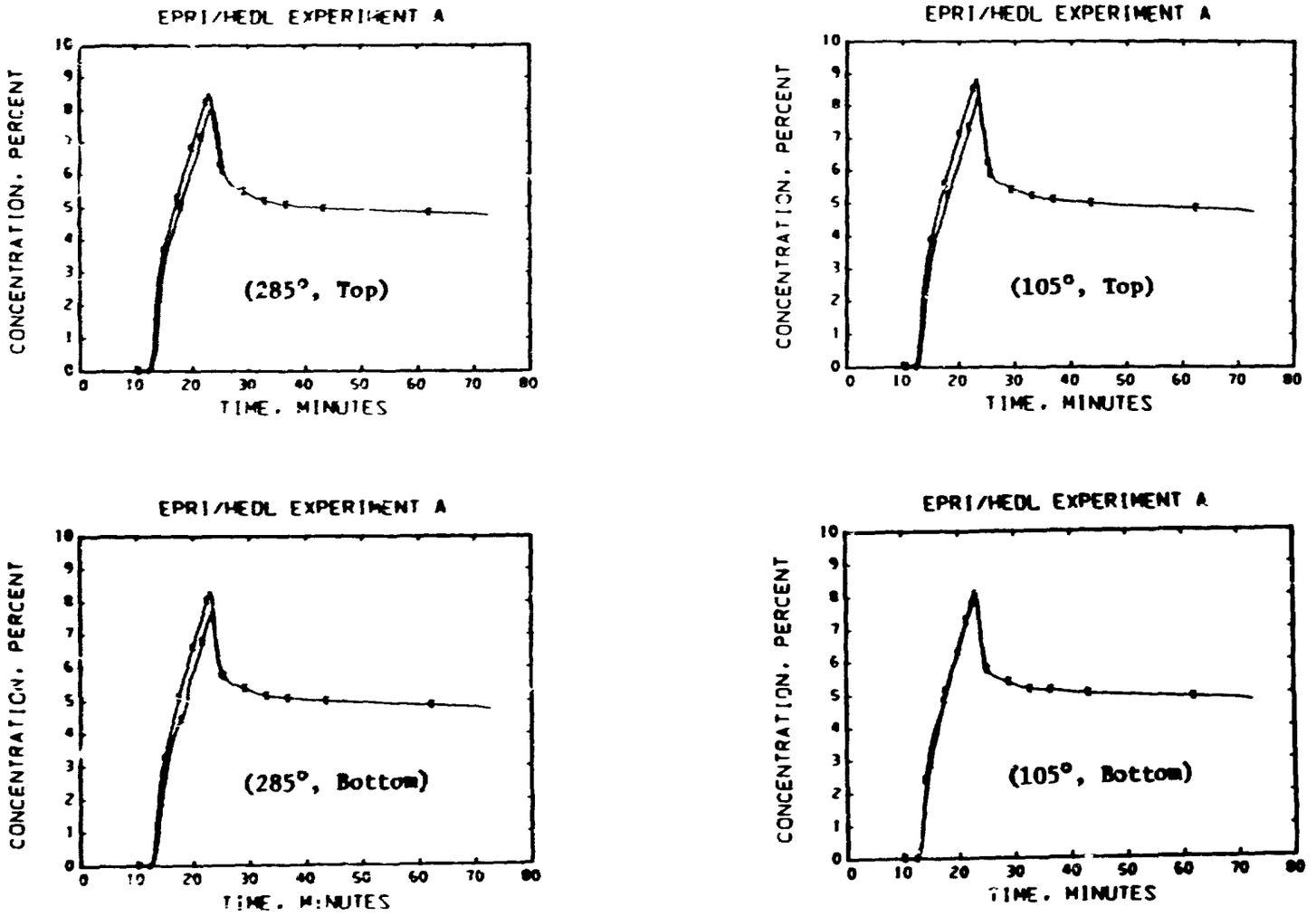

Fig. 3. Hydrogen concentrations for Test A on a dry basis for the indicated locations. The Top and Bottom designations are 0.23 m below the ceiling and 0.3 m above the lower deck, respectively. The curves labeled "E" depict experimental data and those labeled "C" represent the blind calculated results.

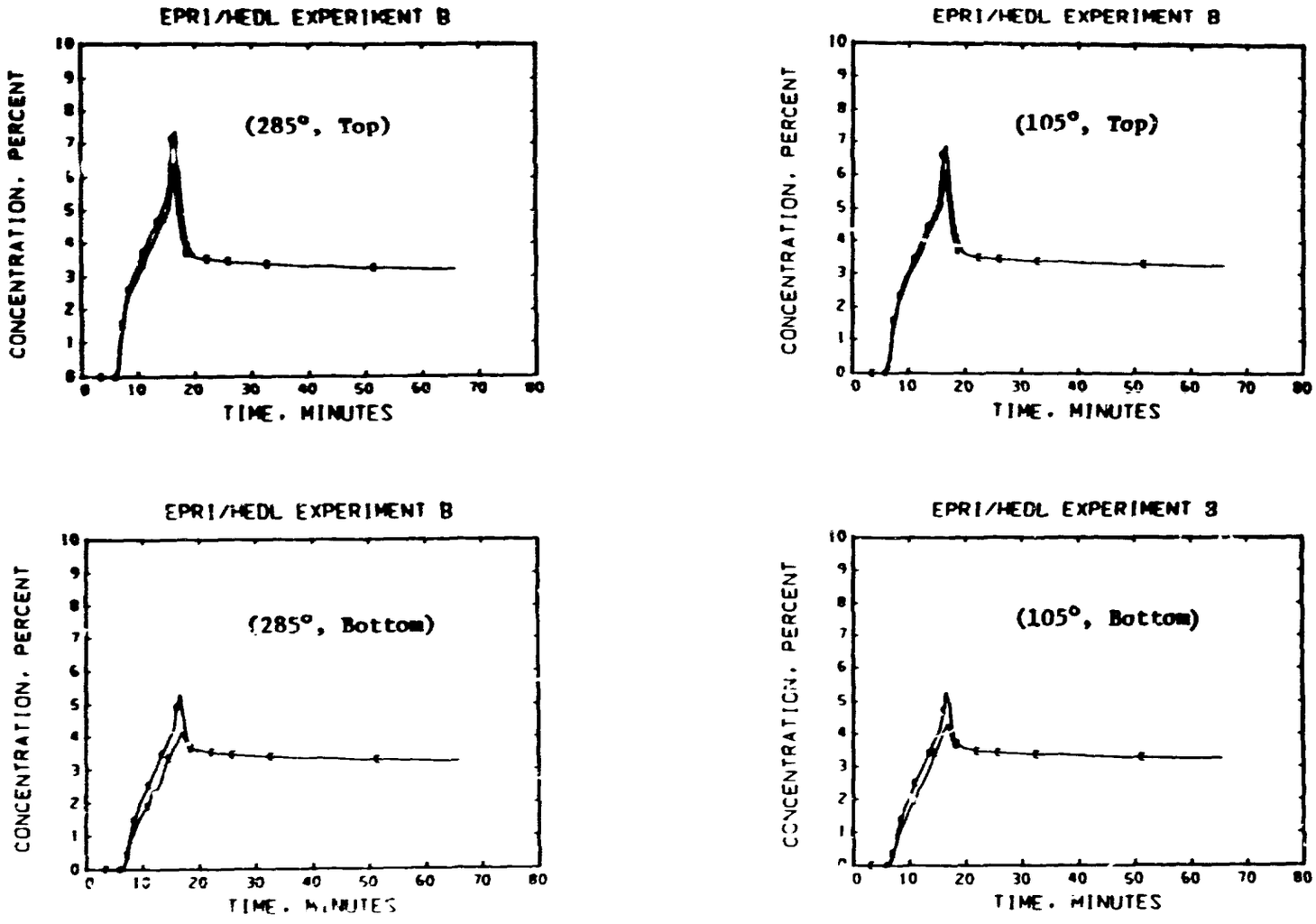

Fig. 4. Helium Concentrations for Test B on a dry basis for the indicated locations. The Top and Bottom designations are 0.23 m below the ceiling and 0.3 m above the lower deck, respectively. The curves labeled "E" depict experimental data and those labeled "C" represent the blind calculated results.

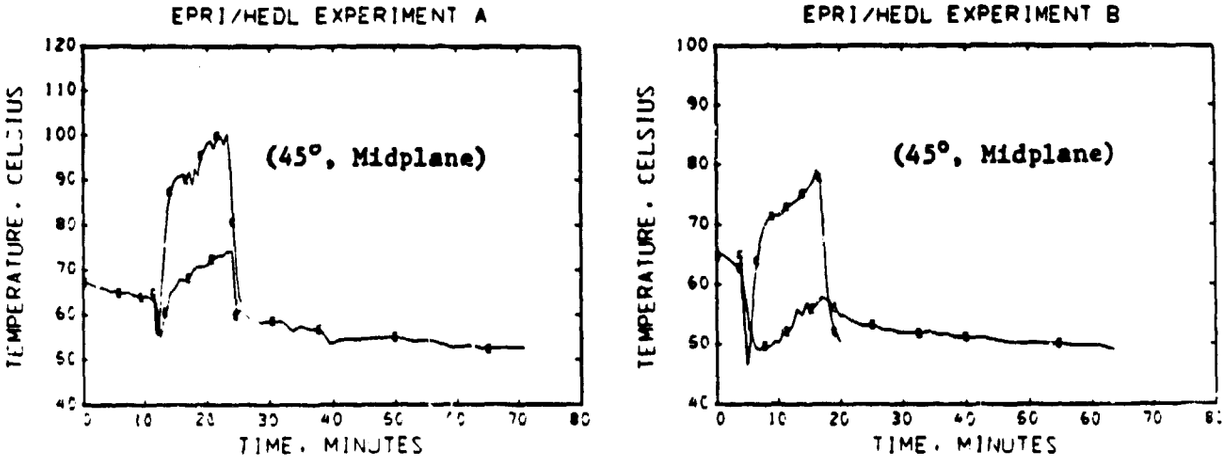

Fig. 5. Compartment temperatures for tests A and B for the indicated locations. The Midplane designation is 2.36 m above the lower deck. The curves labeled "E" depict experimental data and those labeled "C" represent the blind calculated results.

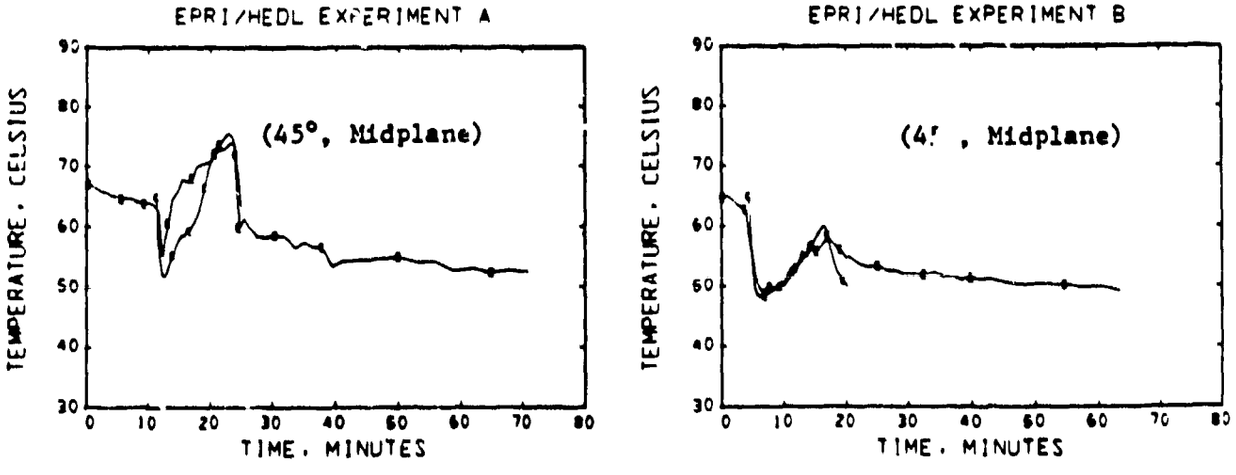

Fig. 6. Compartment temperatures for tests A and B for the indicated locations. The Midplane designation is 2.36 m above the lower deck. The curves labeled "E" depict experimental data and those labeled "C" represent the posttest calculated results.

V. CONCLUSIONS

The mathematical model and solution technique outlined above has proved to be an accurate method for calculating low speed flows with large density variations such as those found in hydrogen mixing within LWR containments. For the time-dependent, fully three-dimensional EPRI/HEDL standard problems, the calculated results compare very closely with the test data even with a fairly coarse computing mesh.

ACKNOWLEDGMENTS

It is a pleasure to express appreciation to F. H. Harlow for his helpful and guiding discussions throughout the course of this work. Additional appreciation is expressed to L. R. Stein and M. D. Torrey for their help in writing the computer programs and to N. C. Romero for his help in producing the graphics. This work was performed under the auspices of the United States Nuclear Regulatory Commission.

References

1. F. H. Harlow and A. A. Amsden, "Numerical Fluid Dynamics Calculation Method for All Flow Speeds," J. Comput. Phys. 8, 197 (1971).

2. C. K. Forester and A. F. Emergy, "A Computational Method for Low Mach Number Unsteady Compressible Free Convective Flows," J. Comput. Phys. 10, 497 (1972).

3. G. R. Bloom and S. W. Claybrook, "Standard Problems on Hydrogen Mixing and Distribution," Westinghouse Hanford Company, Richland, Washington, March 26, 1982.

4. J. R. Travis (in preparation), "A Finite-Difference Method for Time-Dependent, Three-Dimensional Low-Speed Gas Flows with Large Density Variations," Los Alamos National Laboratory report.

5. G. R. Bloom, L. D. Muhlestein, and A. K. Postma, "Hydrogren Distribution in a Compartment with a High Velocity Hydrogen-Steam Source," Second International Workshop on the Impact of Hydrogren on Water Reactor Safety, Albuquerque, NM, October 1982.

6. J. R. Travis, Letter to G. R. Bloom and S. W. Claybrook submitting standard problem results, April 27, 1982.

7. H. Uchida, A. Ogama, and Y. Togo, "Evaluation of Postincident Cooling Systems of Light-Water Power Reactors," Proc. of the Third Inter. Conf. on the Peaceful Uses of Atomic Energy, Geneva, Switzerland (August 31 - Sept. 9, 1964); Vol. 13, 93-104, United Nations, A/CONF.28, p. 436 (1965).